Self-Organizing Artificial Intelligence Captures Landscape Changes Correlated with Human Impact Data

John Mwangi Wandeto, Birgitta Dresp

Preprint

Self-Organizing Artificial Intelligence Captures Landscape Changes Correlated with Human Impact Data

John M. Wandeto[1], Birgitta Dresp-Langley[2]*

[1] Department of Information Technology, Dedan Kimathi University of Technology, Nyeri, Kenya
[2] Centre National de la Recherche Scientifique UMR 7357 ICube Lab, Strasbourg University, France; birgitta.dresp@unistra.fr
* Correspondence: birgitta.dresp@cnrs.fr; Tel.: +33-388119117

Abstract: Self-organization is the core principle of all learning in Adaptive Resonance Theory (ART), which has been highly successful in accounting for biological visual learning, or biologically plausible computational modelling of visual processing. Such processing includes the analysis of visual data we may not be able to see consciously, such as changes in fine visual detail in images relating to alterations in natural or urban landscapes, for example. In the course of time, such imaging data may reveal structural changes that are the consequence of measurable human impact or climate change. Capturing such change in time series of satellite images before the human eye can see them makes them available at early stages to citizens, professionals, and policymakers, promotes change awareness, and facilitates early decision making for action. Here, we use unsupervised Artificial Intelligence (AI) that exploits principles of self-organized biological visual learning for the analysis of time series of satellite images. The Quantization Error (QE) in the output of a Self-Organizing Map prototype is exploited as a computational metric of variability and change. Given the proven sensitivity of this neural network metric to the intensity and polarity of image pixel contrast, and its proven selectivity to pixel colour, it is shown to capture critical changes in urban landscapes. This is achieved here in the example of satellite images from two regions of geographic interest in Las Vegas County, Nevada, USA across the years 1984-2008. The SOM-QE analysis is combined with the statistical analysis of demographic data revealing human impacts correlated with the structural changes in the specific regions of interest. By correlating the impact of human activities with the structural evolution of urban environments we further expand SOM-QE analysis, as a parsimonious and reliable AI approach, to the rapid detection of human footprint-related environmental change.

Keywords: SatelliteImages, Landscapes, Urban Environment, Las Vegas, Self Organizing Map (SOM), Quantization Error, Demographic Data, Human Impact

1. Introduction

Grossberg's Adaptive Resonance Theory proposes neural network models that enable stable brain learning in non-stationary and unexpected worlds [1]. These models rely on self-organized learning akin to biological synaptic learning [2, 3, 4]. In biological neural networks, such learning is by nature unsupervised and may be accounted for in terms of competitive *winner-takes-all* matching principles [5]. The Self-Organizing Map (SOM) is, by comparison with the ART models, a parsimonious, one may call it minimalist, artificial neural network architecture [6, 7] with input-driven self-organization using *winner-takes-all* learning in sensory model neurons that become locally and globally ordered during learning. In our previous studies, we exploited the functional properties of sensitivity to spatial extent, intensity, and colour of local pixel contrasts of the

Quantization Error (QE) in the output of a SOM for automatic data classification as a function of finest, mostly invisible, yet, clinically or functionally relevant, local variations in visual or other data time series. This work, extensively and well documented in our prior publications [8-19], has permitted establishing SOM-QE [8] as a reliable computational model of statistical variability in sensed data, directly relating to critical local changes in images of one and the same landscape [15], of organs [19], cells [10, 13, 16], and other simulated visual objects at different moments in time [11, 14, 17, 18], and in temporal series of sensor responses from surgical data simulating robotic control by grip forces distributed in the human hands of experts and novices [9, 12].

Any technique for the determination of the finest changes of visual or other sensed data across time, even when combined with an advanced imaging model, sooner or later requires human classification for an interpretation. This may involve guesswork when the spatiotemporal uncertainty [20-22] in the data or visual image contents is high. It then becomes difficult to rule out subjectivity of the analyst, even when the latter is a skilled expert. To ensure quality decision making, affordable precision software for automatic data classification should combine high accuracy with further advantages relative to speed, objectivity, and reproducibility of the classification. All these have been proven ensured by SOM-QE within the scope of its application [8]. In this work here, we show simulations exploiting SOM-QE analysis [8] to demonstrate its statistically significant sensitivity to the spatial extent of local pixel contrast translating significant landscape changes correlated with significant increase in human impact, and its ecological footprint as a consequence [23], in response to these changes. NASA Landsat images of Las Vegas City Centre and the residential North of Las Vegas from a time period between 1984 and 2008 were submitted to SOM-QE analysis for this study. In the 1980ies Las Vegas City, located in the middle of the Nevada Desert, featured mainly 'The Strip', with a number of smaller casinos and motels. Subsequently, in a large restructuration project between 1990 and 2007 a large number of the old casinos and motels were demolished. The ensuing reconstruction of Las Vegas City Centre and the subsequent opening of a large number of mega-resorts with casino spaces, tropical landscapes with waterfalls or simulations of urban environments such as Venice, restaurants with world-class chefs, and shows performed by international megastars like Celine Dion transformed Las Vegas City Centre and The Strip entirely. By offering multiple kinds of entertainment, dining gambling, and lodging, attracting millions of visitors from all over the world, Las Vegas City Centre has become one of the largest entertainment poles in the world [24]. Most elements of the project opened in late 2009. This was accompanied by the rapid spread of greater Las Vegas, including the residential North, into the adjacent desert. The population count grew from thousands in 1984 to millions in 2009.

2. Materials and Methods

25 satellite images of the geographic regions of interest (ROI), Las Vegas City Center and Residential North were pre-processed and then submitted to SOM-QE analysis. The original pre-processed input images can be accessed from the Supplementary Materials.

2.1. Image input

The original images were extracted from time-lapse animations of Las Vegas County, Nevada, for a reference time period from 1984 to 2008, as captured by NASA Landsat sensors [25]. VLC [26], an open source media player, was used to generate static images from the time-lapse animations provided. The images are colour-coded for optimal visualization [27], displaying arid desert regions in brownish-gray, building structures in dark-gray and healthy vegetation and green spaces in red pixels. Water is represented by black pixels. Sample copies of two of the pre-processed 25 images for each ROI, Las Vegas City centre (Fig.1) and residential North (Fig. 2) from the years 1984 and 2008 are shown here below.

Figure 1. Representation of two of the 25 satellite image extracts of Las Vegas city centre in 1984 (left) and 2008 (right), after preprocessing.

Figure 2. Representation of two of the 25 satellite image extracts of Las Vegas residential North in 1984 (left) and 2008 (right), after preprocessing.

Before running the SOM-QE analysis on the image time series for the two geographic ROI, the images were pre-processed to ensure they are all identically scaled and aligned within a given series. This was achieved by applying the method of co-registration using *StackReg* [28], which is a plug-in for *ImageJ*, an open source image processing program designed for scientific multidimensional image processing. The last image of the time series was used to anchor the registration. Control for variations in contrast strength between images of a given series was performed after registration. This was achieved by increasing the image contrast and by removing any local variations at different times of image acquisition [29-30]. For each extracted image, contrast intensity (I) normalization was ensured using

$$I_{final} = (I - I_{min}/I_{max} - I_{min}) \text{x} 255 \qquad (1)$$

The registered and normalized image taken in 2008 from each ROI was used to train the SOM. Since the original images used colour to emphasize different areas on the maps, pixel-based RGB values are used as input features to the SOM. This ensures a pixel-by-pixel capture of detail and avoids errors due to inaccurate feature calculation, which often occurs with complex images [30].

2.2. SOM-QE analysis

The Self-Organizing Map (the prototype for this study here is graphically represented in Fig. 3, for illustration) may be described formally as a nonlinear, ordered, smooth mapping of high-dimensional input data onto the elements of a regular, low-dimensional array [6, 7, 8]. It is assumed that the set of input variables can be defined as a real vector x, of n-dimensionality. A parametric real vector m_i of n-dimension is associated with each element in the SOM. Vector m_i is a model and the SOM is therefore an array of models. Assuming a general distance measure between x and m_i denoted by $d(x, m_i)$, the map of an input vector x on the SOM array is defined as the array element m_c that matches best (smallest $d(x, m_i)$) with x. During the learning process, the input vector x is compared with all the m_i in order to identify m_c. The Euclidean distances $||x-m_i||$ define m_c. Models topographically close in the map up to a certain geometric distance indicated by h_{ci} will activate each other to learn something from their common input x.

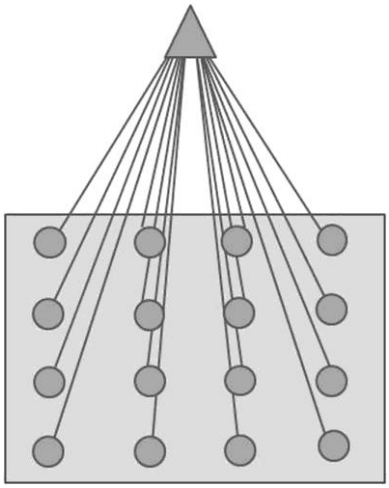

Figure 3. Graphic representation of the 4x4 SOM prototype with 16 models, indicated by the filled circles in the grey box. Each of these models is compared to the SOM input in an unsupervised winner-take-all learning process. The input vector corresponds to the RGB image pixel space.

This results in a local relaxation or smoothing effect on the models in this neighborhood, which in continuous learning leads to global ordering. Self-organized learning in a SOM is represented by the equation

$$\boldsymbol{m(t+1) = m_i(t) + \alpha(t) h_{ci}(t)[x(t) - m_i(t)]} \quad (2)$$

where $\boldsymbol{t = 1, 2, 3}$...is an integer, the discrete-time coordinate, $h_{ci}(t)$ is the neighborhood function, a smoothing kernel defined over the map points which converges towards zero with time, $\boldsymbol{\alpha(t)}$is the learning rate, which also converges towards zero with time and affects the amount of learning in each model. At the end of the *winner-take-all* learning process in the SOM, each image input vector x becomes associated to its best matching model on the map m_c. The difference between x and m_c, $||x - m_c||$, is a measure of how close the final SOM value is to the original input value and is reflected by the quantization error QE. The average QE of all Xi in an image is given by

$$\boldsymbol{QE = 1/N \sum_{i=1}^{N} \left\| X_i - m_{c_i} \right\|} \quad (3)$$

where N is the number of input vectors x in the image. The final weights of the SOM are defined by a three dimensional output vector space representing each R, G, and B channel. The magnitude as well as the direction of change in any of these from one image to another is reliably reflected by changes in the QE. The SOM training process consisted of 1 000 iterations for a two-dimensional rectangular map of 4 by 4 nodes capable of creating 16 model observations from the data. The spatial locations, or coordinates, of each of the 16 models or domains, placed at different locations on the map, exhibit characteristics that make each one different from all the others. When a new input signal is presented to the map, the models compete and the winner will be the model the features of which most closely resemble those of the input signal. The input signal will thus be classified or grouped in one of models. Each model or domain acts like a separate decoder for the same input, i.e. independently interprets the information carried by a new input. The input is represented as a mathematical vector of the same format as that of the models in the map. Therefore, it is the presence or absence of an active response at a specific map location and not so much the exact input-output signal transformation or magnitude of the response that provides the interpretation of the input. To obtain the initial values for the map size, a trial-and-error process was implemented. Map sizes larger than 4 by 4 produced observations where some models ended up empty, which meant that these models did not attract any input by the end of the training. As a consequence, 16 models were sufficient to represent all the fine structures in the image data. Neighborhood distance and learning rate were constant at 1.2 and 0.2 respectively. These values

were obtained through the trial-and-error method after testing the quality of the first guess, which is directly determined by the value of the resulting quantization error; the lower this value, the better the first guess. It is worthwhile pointing out that the models were initialized by randomly picking vectors from the training image. This allows the SOM to work on the original data without any prior assumptions about any level of organization within the data. This, however, requires starting with a wider neighborhood function and a higher learning-rate factor than in procedures where initial values for model vectors are pre-selected. The approach is economical in terms of computation times, which constitutes one of its major advantages for rapid change *versu*s no change detection on the basis of even larger sets of image data, prior to any further human intervention or decision making. The last image of the series from the time range here was used to train the SOM. After training, SOM-QE analysis permits determining the QE in the map output for each of the 25 images of the series. The code used for implementing the SOM-QE is available in the "R-badged articles" series [8] of the journal *Software Impacts*, a collection that presents software publications that have been verified for computational reproducibility by CodeOcean, a cloud-based computational reproducibility platform that helps the community by enabling sharing of code and data as a resource for non-commercial use. Certified papers have an attached Reproducibility Badge, a permanent Reproducibility Capsule, and are listed on the CodeOcean website [8].

3. Results

The results from the SOM-QE analysis on the image time series for the two ROI are given in Table 1 as a function of the image the year was taken and the type of ROI. They show a general trend towards increase in the QE metric across images for each ROI between 1984 and 2008. The QE in the SOM output is a reliable indicator of variability in pixel color (or contrast intensity; here in this study all images were normalized for contrast intensity and did not display variability across images) as shown in our previous work.

Table 1.SOM-QE output as a function of the image year and geographic ROI.

Year	Las Vegas City	Residential North
1984	0,240437503	0,151226618
1985	0,264341069	0,157865360
1986	0,271480118	0,155998180
1987	0,289065099	0,169213765
1988	0,282803632	0,210600120
1989	0,286535270	0,213982186
1991	0,303956828	0,219973707
1991	0,298541690	0,225406972
1992	0,301994751	0,214975264
1993	0,293683986	0,208605453
1994	0,304328745	0,221313177
1995	0,298240329	0,212630331
1996	0,309779114	0,222464495
1997	0,284870821	0,225816809
1998	0,291493024	0,223026329
1999	0,296067339	0,238731572
2000	0,304491317	0,246826836
2001	0,311488540	0,254509105

2002	0,314104190	0,259835794
2003	0,299101833	0,263285485
2004	0,299139369	0,249477866
2005	0,296761075	0,237934169
2006	0,305053585	0,250044464
2007	0,301298833	0,256201407
2008	0,314321877	0,261825498

Here, the increase in QE captures the increasing structural variability of the landscapes, directly reflected by an increasing variability in image pixel colors, across these critical years of restructuration of Las Vegas City accompanied by the progressive building development of the Residential North. In a first analysis, these data were submitted to linear regression analysis to assess the statistical significance of the increase in QE across the years.

3.1. Linear regression and statistical trend analysis on the QE data

The linear fits to the trend in the QE to increase across the image years are shown in Figure 4.

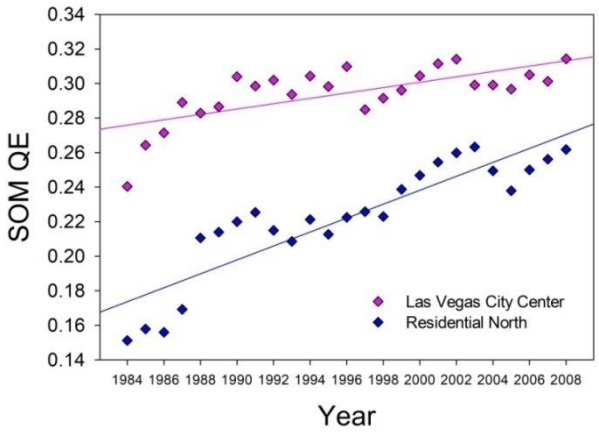

Figure 4. Linear fits to the QE data as a function of the year in which a study image for a given ROI was taken.

As an estimate of the part of variance in the data that is accounted for by a linear trend, or fit, the regression coefficient r^2 is a direct reflection of the goodness of that fit. The statistical significance of the trend in the data in any given direction, upward or downward, is determined by the probability that the linear adjustment sufficiently differs from zero on the basis of Student's distribution (t). The results from the comparison QE *versus* year of image acquisition reveal a statistically significant linear trend towards increase in *QE* as a function of time for both ROI.The results from the linear regression analysis with the slopes and intercepts of the fits and their regression coefficients r^2 are shown in Table 2. The results from the statistical trend analyses with Student's t, Degrees of Freedom (DF) for a given comparison and the associated probability (p), limits are given in Table 3.

Table 2. Fit parameters from the linear regression analysis of the QE data as a function of the geographical ROI.

Linear Fit Parameter	Las Vegas City	Residential North
Slope (b_1)	1,554	4,0331
Intercept (b_0)	-2,8077	-7,8286
r^2	0,4776	0,7995

Table 3. Trend statistics as a function of the geographical ROI.

Trend Parameter	Las Vegas City	Residential North
t	88,98	33,45
DF	(1, 24)	(1, 24)
p	<.001	<.001

The regression coefficients r^2(Table 2) reveal that the linear fit to the QE data for the images of the residential North is a reasonably good one, while the linear model poorly fits the QE data for the images of Las Vegas City. This is consistent with the type of structural change that took place in each of the ROI across the study years. There was a step-by-step reorganization of the City Center, with old casinos and hotel centers disappearing one after the other to be replaced by new ones, and a much smoother, rather progressive development of buildings the in desert regions that have become part of what is now the residential North. The linear trend statistics (Table 3) reveal a statistically highly significant increase in the QE data across the image years for both ROI.

3.2. Human impact data

For the reference time period of this study, the Las Vegas Convention and Visitors Authority [31], and the Las Vegas Population Review [32] have provided publically archived data that show the increase of human impact across the same years as those from which the satellite images analyzed here were taken. These data are shown in Table 4 in terms of annual population estimates in thousands for Greater Las Vegas, which includes the City and the residential North, and visitors *per annum* in millions.

Table 4. Human impact data across the years in terms of visitor (in millions) and population (in thousands) estimates *per annum.*

Year	Visitors (in millions)	Population (in K)
1984	12,8000	191,0000
1985	14,2000	197,0000
1986	15,2000	204,0000
1987	16,2000	226,0000
1988	17,2000	240,0000
1989	18,1000	266,0000
1991	20,9000	276,0000
1991	21,3000	298,0000
1992	21,9000	310,0000
1993	23,5000	330,0000
1994	28,2000	352,0000
1995	29,0000	374,0000
1996	29,6000	406,0000
1997	30,4000	423,0000
1998	30,6000	448,0000
1999	33,8000	466,0000
2000	35,8000	483,0000
2001	35,0000	506,0000

2002	35,0000	521,0000
2003	35,5000	535,0000
2004	37,3000	560,0000
2005	38,6000	576,0000
2006	38,3000	592,0000
2007	37,5000	603,0000
2008	39,5000	608,0000

These data, shown graphically in Figure 5, were also submitted to linear regression and statistical trend analysis.

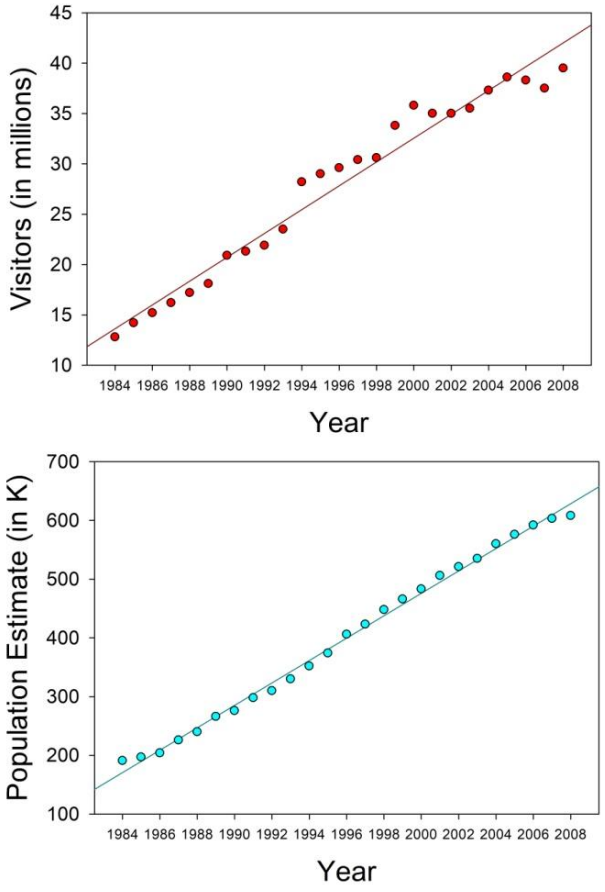

Figure 5. Linear fits to the human impact data as a function of the year in which the study images were taken.

3.3. Linear regression and statistical trend analysis on the human impact data

The results from the comparisons population estimate *versus* year of image acquisition and annual visitor estimate *versus* year reveal statistically significant linear trends towards increase as a function of time for both types of human impact data.The linear fits to the trends in these data to increase across the image years are shown in Figure 5. The results from the linear regression analysis with the slopes and intercepts of these fits and their regression coefficients r^2 are shown in Table 5. The results from the statistical trend analyses with Student's *t*, Degrees of Freedom (DF) for a given comparison and the associated probability (*p*), limits are given in Table 6.

Table 5. Fit parameters from the linear regression analysis of the human impact data in terms of visitors in millions and population (residents) in thousands *per annum*.

Linear Fit Parameter	Visitors	Population
Slope (b_1)	1,1828	19,0723
Intercept (b_0)	-2,333	-3766
r^2	0,9657	0,9955

Table 6. Trend statistics as a function of the type of human impact data

Trend Parameter	Visitors	Population
t	15,70	14,20
DF	(1, 24)	(1, 24)
p	<.001	<.001

The regression coefficients r^2(Table 5) reveal that the quality of the linear fits to the human impact data across the years is excellent. The steady increase in population and visitors of Greater Las Vegas is consistent with the restructurations that took place across these years, creating an increasingly larger offer for state-of-the-art entertainment on the one hand, and a need for more residential development catering for the needs of people providing their workforce for this expanding industry. The linear trend statistics (Table 6) reveal a statistically highly significant increase in the visitors and population data across these critical years.

3.4. Correlation Analysis

In the next analysis, the correlations between the QE distributions from the SOM-QE analysis and the distributions reflecting human impact data in terms of population and visitors *per annum* statistics and were computed. Correlations are useful because they may indicate a predictive relationship between variables, which then can be further exploited in practice. To that effect we computed Pearson's correlation coefficient *R*, which mathematically determines statistical covariance. The probability *p* that the covariance of two observables is statistically significant is determined by the magnitude of the Pearson coefficient, which is directly linked to the strength of correlation, while its sign is directly linked to the direction of the covariance (positive or negative) of two variables. This analysis was performed on the paired distributions for the QE from the image analysis of the residential North as a function of the population data and for the results from the image analysis of Las Vegas City as a function of the average yearly visitor estimates. The results show statistically significant positive correlations between the paired variables in both cases. The correlation statistics, with the Pearson coefficients for a given comparison and the associated DF and probability limits, are shown in Table 7.

Table 7. Pearson correlation statistics as a function of the type of comparison

Correlation Parameter	QE North *vs* Population	QE City *vs* Visitors
Pearson's *R*	0,87	0,71
DF	(1, 24)	(1, 24)
p	<.001	<.001

The correlations were plotted graphically for visualization (Figure 6), showing the SOM-QE from the 25 images of the residential North as a function of the yearly population estimates

(Fig. 6, top) and the SOM-QE from the 25 images of Las Vegas City as a function of the annual number of visitors across the years of the reference period (Fig. 6, bottom).

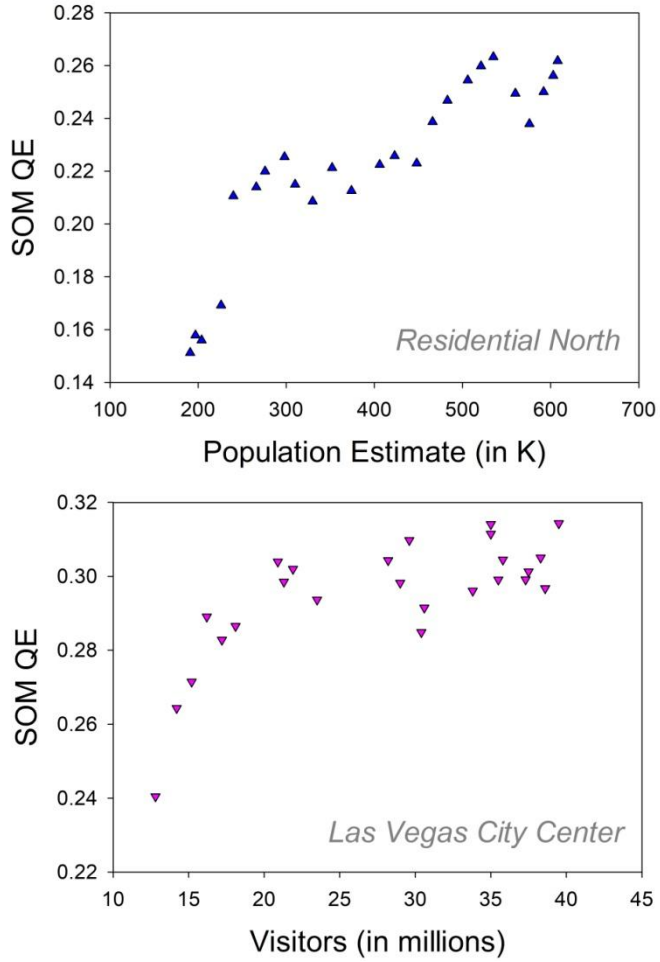

Figure 6. Correlation between the QE values from the image analyses and the pertinent human impact estimate for a given geographic ROI.

4. Discussion

This study is couched in the larger framework of pixel colour-based approaches to the analysis of Earth images from satellites such as Landsat to study temporal changes relating to the effects of human activities on landscape changes and/or climate change [33, 34]. Here, the SOM-QE data from analyses of satellite images of the residential North of Greater Las Vegas and the Las Vegas City Center consistently capture the anthropogenic structural changes in each ROI across the study years. The step-by-step reorganization of the City Center, with old casinos and hotel centers disappearing and replaced by more and larger new ones, and the progressive development of housing and infrastructure in desert regions that are now part of the residential North. The significant positive correlations between the QE distributions from the SOM-QE analysis and the distributions reflecting human impact data in terms of population and visitors *per annum* allow for adeeper analysis of anthropogenic movements across these critical years. The steady increase in visitors of Las Vegas City reflects the direct anthropogenic response to the increasingly larger offer of state-of-the-art entertainment in the City. This engendered an increasing need for residential development in desert regions to provide housing for an increasing population providing the necessary workforce. During these same years, the water supply to these regions dwindled away progressively, as shown in a previous study applying SOM-QE to satellite images of Lake Mead,

the major source of water supply to greater Las Vegas, which includes the residential North, and Las Vegas City. These observations reveal combined effects of climate change and increase in human footprint [35] on this region, bearing in mind that greater Las Vegas is one of the driest regions in the world [36]. The analyses provided here open a window for understanding the links between economic development and environmental impact in this particular region. When plotting the total revenues from gaming and leisure activities [37] of Las Vegas City Centre ('The Strip') and the water level statistics for Lake Mead provided by the Hoover Dam Control Room [38] across the years of the reference period (for illustration only here), we see a negative correlation (Pearson's R (1,24) = -0,82; p<.00) between economic development and resource availability (Figure 7).

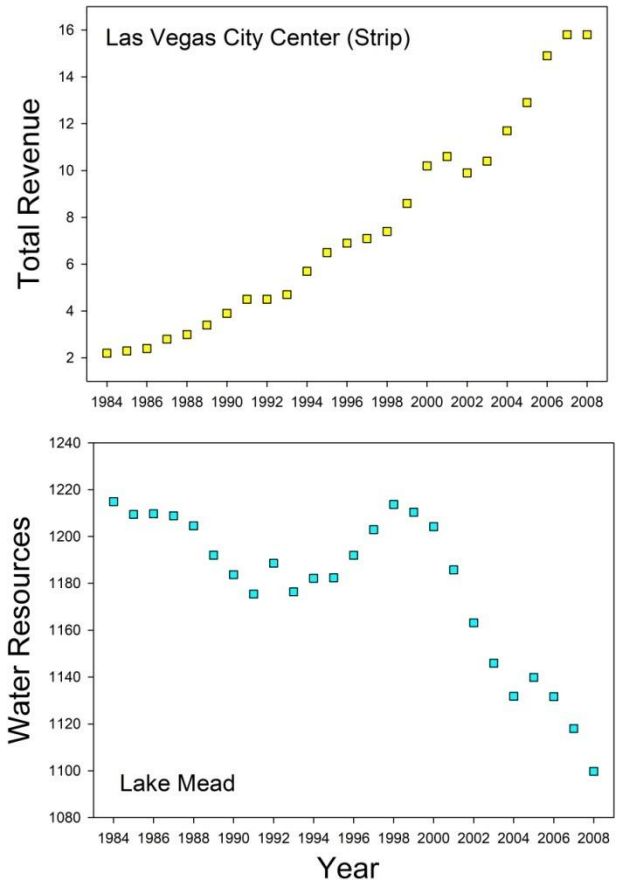

Figure 7. Revenues from gaming and leisure activities (top) and water level statistics for Lake Mead across the years of the reference study.

The results from this study highlight some novel aspects of the full potential of input-driven self-organization in a parsimoniously designed neural network model (AI). SOM-QE provides a highly reliable output metric that scales, in a few minutes and with a to-the-single-pixel precision, local variability in time series of images containing millions of pixels each. Although it is self-organizing, learning in the SOM is explainable and so are its prototype design architecture and the neural workspace. The input data are not biased, and clearly defined physically. The output metric, the QE, initially used as a quality metric and for network quantization [6, 7], is proven a powerful and consistent detector of invisible local changes. When the input to a SOM is constant across time, the QE metric is invariant [6, 7]. When variability in a locally defined dimension of the input data is systematic across time, in a given direction (increase or decrease), the QE will systematically and reliably increase or decrease, as shown in the bulk of our previous work and, once again, here in this

study. Easily implemented, fast, and computationally economic, SOM-QE satisfies all the current criteria for trustworthy and sustainable AI [39, 40], within a modest but diverse range of applications.

Supplementary Materials: The following are available online at www.mdpi.com/link: Folder S1, 50 original pre-processed images from the time series of 25 images for each the two ROI.

Funding: This research received no external funding.

Acknowledgments: The authors gratefully acknowledge support from their respective host institutions.

Conflicts of Interest: The authors declare no conflict of interest.

References

1. Grossberg S. Conscious Mind, Resonant Brain: How Each Brain Makes a Mind 2021, Oxford University Press.
2. Hebb, D. *The Organization of Behaviour* 1949; John Wiley & Sons: Hoboken, NJ, USA.
3. Grossberg, S. Self-organizing neural networks for stable control of autonomous behavior in a changing world. In *Mathematical Approaches to Neural Networks*; Taylor, J.G., Ed.; Elsevier Science Publishers: Amsterdam, The Netherlands, 1993; pp.139–197.
4. Dresp-Langley, B. Seven Properties of Self-Organization in the Human Brain. *Big Data Cogn Comput* 2020; 4, 10.
5. Carpenter, GA. Distributed Learning, Recognition, and Prediction by ART and ARTMAP Neural Networks. *Neural Netw* 1997; 10(8), 1473-1494.
6. Kohonen T. *Self-Organizing Maps*. **2001**; online: http://link.springer.com/10.1007/978-3-642-56927-2
7. Kohonen T. MATLAB Implementations and Applications of the Self-Organizing Map. *Unigrafia Oy*, **2014**; Helsinki, Finland.
8. Wandeto J, Dresp-Langley B. SOM-QE ANALYSIS - a biologically inspired technique to detect and track meaningful changes within image regions. *Software Impacts* 2023; 17, 100568. https://doi.org/10.1016/j.simpa.2023.100568
9. Liu R, Wandeto J, Nageotte F, Zanne P, de Mathelin M, Dresp-Langley, B. Spatiotemporal modeling of grip forces captures proficiency in manual robot control. *Bioengineering* 2023; 10, 59.
10. Dresp-Langley B, Wandeto J. Unsupervised classification of cell-imaging data using the quantization error in a self-organizing map. In: Arabnia, H.R., Ferens, K., de la Fuente, D., Kozerenko, E.B., Olivas Varela, J.A., Tinetti, F.G. (eds.), *Advances in Artificial Intelligence and Applied Cognitive ComputingTransactions on Computational Science and Computational Intelligence*, pp. 201-209, Springer International Publishing, Cham (2021).
11. Dresp-Langley B, Wandeto J. Human symmetry uncertainty detected by a self-organizing neural network map. *Symmetry* 2021; 13, 299.
12. Dresp-Langley B, Liu R, Wandeto J. Surgical task expertise detected by a self-organizing neural network map. *10.48550/arXiv.2106.08995*; 2021.
13. Dresp-Langley B, Wandeto J. Pixel precise unsupervised detection of viral particle proliferation in cellular imaging data. *Informatics in Medicine Unlocked* 2020; 20, 100433.
14. Wandeto J, Dresp-Langley B. The quantization error in a self-organizing map as a contrast and colour specific indicator of single-pixel change in large random patterns. *Neural Networks* 2019; 119, 273-285.
15. Dresp-Langley B, Nyongesa H, Wandeto J. Vision-inspired automatic detection of water level changes in satellite images: the example of Lake Mead. *Perception* 2019; 48, ECVP Abstract Supplement.
16. Wandeto J and Dresp –Langley B. Ultrafast automatic classification of SEM image sets showing CD4 cells with varying extent of HIV virion infection. *7ièmes Journées de la Fédération de Médecine Translationnelle de Strasbourg* 2019; May 25-26, Strasbourg, France.
17. Wandeto J, Dresp-Langley B. The quantization error in a self-organizing map as a contrast and colour specific indicator of single-pixel change in large random patterns. *Neural Networks (Special Issue in Honor of the 80th Birthday of Stephen Grossberg)*, 2019; 120, 116-128.
18. Wandeto J, Nyongesa H, Dresp-Langley, B. Detection of smallest changes in complex images comparing self-organizing map to expert performance. *Perception* 2017; 46, ECVP Abstract Supplement.

19. Wandeto J, Nyongesa H, Rémond Y, Dresp-Langley B. Detection of small changes in medical and random-dot images comparing self-organizing map performance to human detection. *Informatics in Medicine Unlocked* 2017; 7, 39-45.
20. Cattell JM. The influence of the intensity of the stimulus on the length of the reaction time. *Brain.* 1886;8: 512-515.
21. Exner S. Ueber die zu einer Gesichtswahrnehmung noetige Zeit. *Sitzungsberichte der Kaiserlichen Akademie der Wissenschaften,* 1868; 57:601-632.
22. Green, DM, Swets, JA. *Signal detection theory and psychophysics*. 1973; Krieger Publishing, Huntington, NY.
23. Dou X, Guo H, Zhang L, Liang D, Zhu Q, Liu X, Zhou H, Lv Z, Liu Y, Gou Y, Wang Z. Dynamic landscapes and the influence of human activities in the Yellow River Delta wetland region. *Sci Total Environ* 2023; 899, 166239. doi: 10.1016/j.scitotenv.2023.166239.
24. Luke, TW. Gaming space: casinopolitan globalism from Las Vegas to Macau. In Steger, M., McNevin, A. (eds.) *Global Ideologies and Urban Landscapes*, Routledge, 2013; pp. 77-87.
25. NASA/Goddard Space Flight Center Landsat images from USGS Earth Explorer. ID: 10721, Mar. 2012: http://svs.gsfc.nasa.gov/10721 last accessed 2023/09/11.
26. The VLC media player source code: https://www.videolan.org/vlc/download-sources.html last accessed 2023/09/19.
27. Dresp-Langley, B, Reeves, A. Colour for behavioural success. *i-Perception*. 2018; 9(2): 1–23.
28. Thévenaz P, Ruttimann UE, Unser MA. Pyramid Approach to Subpixel Registration Based on Intensity. *IEEE Transactions on Image Processing* 1998; 7, 27–41.
29. Wieland M, Pittore M. Performance Evaluation of Machine Learning Algorithms for Urban Pattern Recognition from Multi-spectral Satellite Images. *Remote Sensing* 2014; 6, 2912–2939.
30. Schneider CA, Rasband WS, Eliceiri KW. From NIH Image to ImageJ: 25 years of image analysis. Nature Methods 2012; 9, 671 (2012).
31. Las Vegas Convention and Visitors Authority, Statistics: https://www.lvcva.com/ last accessed: 2023/09/20.
32. Las Vegas Population Review: https://worldpopulationreview.com/world-cities/las-vegas-population last accessed: 2023/09/20.
33. Orheim O, Lucchitta B. Investigating Climate Change by Digital Analysis of Blue Ice Extent on Satellite Images of Antarctica. *Annals of Glaciology* 1990; 14, 211-215.
34. Furusawa T, Koera T, Siburian R *et al.*Time-series analysis of satellite imagery for detecting vegetation cover changes in Indonesia. *Sci Rep* 2023; 13, 8437 (2023).
35. Camacho C, Palacios S, Sáez P, Sánchez S, Potti J. Human-induced changes in landscape configuration influence individual movement routines: lessons from a versatile, highly mobile species. *PLoS One* 2014; 9(8):e104974. doi: 10.1371/journal.pone.0104974.
36. Frumkin H, Das MB, Negev M, Rogers BC, Bertollini R, Dora C, Desai S. Protecting health in dry cities: considerations for policy makers. BMJ. 2020; 371:m2936. doi: 10.1136/bmj.m2936.
37. University of Nevada Center for Gaming Research Annual Statistics, 2023; online at: https://gaming.library.unlv.edu/reports/NV_departments_historic.pdf
38. US Department of Interior Bureau of Reclamation, Hoover Dam Control Room Statistics: https://www.usbr.gov/lc/region/g4000/hourly/mead-elv.html last accessed: 2023/10/25.
39. Vetter D, Amann J, Bruneault F. *et al.*Lessons Learned from Assessing Trustworthy AI in Practice. *DISO* 2023;2, 35. https://doi.org/10.1007/s44206-023-00063-1
40. AI HLEG - High-Level Expert Group on Artificial Intelligence. *Assessment List for Trustworthy Artificial Intelligence (ALTAI) for self-assessment* 2020; The European Commission. https://ec.europa.eu/newsroom/dae/document.cfm?doc_id=68342